High Temperature Corrosion of Materials
https://doi.org/10.1007/s11085-024-10280-9

ORIGINAL PAPER

Utilization of Alumina Scale Formation by Ni-Base Alloys for High-Temperature Oxidation and Corrosion Resistance in Harsh Environments

Bingtao Li[1] · **Lee M. Pike**[1]

Received: 19 July 2024 / Revised: 19 July 2024 / Accepted: 21 July 2024

Abstract

High-temperature alloys rely on the formation of a protective oxide scale to resist high-temperature oxidation and corrosion attack, and chromia is the most common oxide to provide this function in commercial alloys. However, certain harsh environments require alloys that utilize the formation of even more protective oxide films to provide improved performance and longer lifetime. In these cases, an alumina scale becomes a viable solution to protect high-temperature alloys. This paper summarizes high-temperature oxidation and corrosion behaviors of several high-temperature Ni- and Co-base alloys tested under various high-temperature conditions, including short-term and long-term oxidation, cyclic oxidation, dynamic (burner rig) oxidation, water vapor oxidation, nitridation, and carburization at temperatures ranging from 871 to 1093 °C (1600–2000°F). The oxidation and corrosion behaviors are compared between the alumina-forming and chromia-forming alloys, and the results show that the alumina-forming alloys were significantly superior to the chromia-forming alloys for high-temperature oxidation and corrosion resistance in terms of oxidation and corrosion rate reduction, scale stability and adhesion, mass penetration suppression, etc. Based on the extensive tests, alumina scales were highly effective in resisting oxidation, nitridation, and carburization attacks, especially under severe oxidation and corrosion conditions. To further demonstrate the benefits of an alumina scale, an alumina-forming alloy with pre-oxidation heat-treatment was also studied in the nitridation test.

Keywords High-temperature oxidation · Nitridation · Carburization · Harsh environment · Alumina (Al_2O_3) scale · Chromia (Cr_2O_3) scale · Ni-base alloys

Extended author information available on the last page of the article

Published online: 30 July 2024

Introduction

Ni- and Co-base alloys are widely used materials in high-temperature applications by virtue of their fabricability, high-temperature strength, and corrosion resistance. The service lifetime of a high-temperature alloy often depends on its ability to resist high-temperature oxidation and corrosion attack, which in turn, relies on the formation of a protective oxide scale. Most commercial alloys utilize the formation of a chromia (Cr_2O_3) scale for oxidation and corrosion resistance when exposed to high-temperature environments. Although chromia scales provide good high-temperature corrosion protection in many applications, their performance can be reduced by factors such as scale thinning due to CrO_3 evaporation, formation of volatile oxidation products in the presence of water vapor, and scale buckling due to development of compressive stresses, to name a few [1–6]. Two specific volatilization reactions involving chromia are:

$$\frac{1}{2}Cr_2O_3 + \frac{3}{4}O_2(g) = CrO_3(g) \tag{1}$$

$$\frac{1}{2}Cr_2O_3 + H_2O(g) + \frac{3}{4}O_2(g) = CrO_2(OH)_2(g) \tag{2}$$

Moreover, many industrial processes are operated in harsh environments, such as extreme temperatures, severe thermal cycling, and aggressive corrosive atmospheres, which require the protective oxide scale to be more stable to resist severe high-temperature oxidation and corrosion attack. To protect alloys in harsh environments, alumina (Al_2O_3) scale could provide great benefits including slow growth kinetic, thermodynamic stability in oxidizing atmospheres, dense scale structure, and good adhesion to resist scale degradation and spallation [7–10]. An alumina scale is thermodynamically more stable than a chromia scale, and alumina scale growth rates are significantly lower than those of chromia scales, such as one to two orders of magnitude slower [6, 10]. The slow kinetics of alumina scales results in a thin oxide scale with less stress development for better scale spallation resistance. Although alumina scales are also impacted by water vapor, studies have shown that the gaseous product from the reaction between alumina and water vapor, $Al(OH)_3$, had significantly lower partial pressure than $CrO_2(OH)_2$ in 1atm atmosphere consisting of 50–50 O_2 and H_2O over the temperature range of 700 to 1500 °C [6]. The aforementioned factors enable the alumina scale as a protective surface layer to provide excellent high-temperature oxidation and corrosion resistance. It is noteworthy that minor alloying elements have profound effects on oxidation behaviors of alloys, particularly reactive elements (RE) on improving alumina scale adhesion for alumina-forming alloys [11, 12].

Many studies have shown that alumina scales offered superior high-temperature corrosion resistance when compared to chromia scales. Barnes and Lai [13] studied high-temperature nitridation of Fe-, Ni-, and Co-base alloys at the temperatures of 649, 982, and 1093 °C in 100% ammonia and showed that 601 and 617 alloys (both have relatively low Al contents) exhibited extensive internal nitridation

(forming AlN) at 982 and 1093 °C, while 214 alloy with 4.5 wt% Al had very little internal nitride formation at the test temperatures. In addition, their results also supported the beneficial effects of nickel (Ni) and cobalt (Co) on nitridation resistance. In high-temperature applications operated in carbon-containing atmospheres, carburization is often a material issue. Formation of an oxide scale on an alloy could resist high-temperature carburization attack because of negligible permeation of carbon through perfect dense oxide layers, including Cr_2O_3 and Al_2O_3 [14]. However, some carbon permeation is often observed, likely due to pores, fissures, and/or cracks evolved in oxide scale. In a carburization study of high-temperature alloys [15], the alumina-forming 214 alloy was found to be the most resistant to carburization attack, which was attributed to the formation of an alumina scale on the alloy to impede carbon diffusion into the underlying metal.

Although the benefits of alumina scales appear to be substantial, there are limited high-temperature alumina-forming alloys on the market due to fabrication challenges, notably welding. In addition to HAYNES® 214® alloy, Haynes has recently developed two new Ni-base alumina-forming alloys, HAYNES® 233® alloy and HAYNES® HR-224® alloy. Extensive high-temperature oxidation and corrosion studies have been conducted on the alloys. This paper presents high-temperature oxidation and corrosion-resistant behaviors of Haynes' Ni-base alumina-forming alloys under extreme high-temperature conditions by comparing with other widely used Ni- and Co-base chromia-forming alloys. The high-temperature oxidation and corrosion tests conducted include static oxidation, long-term oxidation, cyclic oxidation, dynamic (burner rig) oxidation, water vapor oxidation, nitridation, and carburization.

Experimental Procedures

High-temperature oxidation and corrosion behaviors of Ni-base alumina-forming HAYNES® 214®, HAYNES® 233®, and HAYNES® HR-224® alloys were compared to Ni-base chromia-forming HAYNES® 230®, 617, 625, HASTELLOY® X alloys, and a Co-base HAYNES®[1] 188 alloy. Their nominal alloy compositions are listed in Table 1. Among the alloys studied, 214, HR-224, and 233 alloys contain 4.5, 3.8, and 3.3 wt% Al, respectively, being considered as alumina-forming alloys. The other alloys contain 21–22 wt% Cr to be chromia-forming alloys. Although 617 alloy contains 1.2 wt% Al, it relies on the formation of a chromia scale for high-temperature corrosion resistance. It is noted the reactive elements, such as Zr, Y, and/or La, are added to the alloys except for 617, X, and 625 alloys.

The test coupons were in the mill-annealed condition, and they were cut in size of 25.4 mm × 25.4 mm × (1.3–3.2) mm (1″ × 1″ × 0.050–0.125″) and polished with 120-grit SiC paper to have surface roughness of average 1 μm Ra. For the high-temperature oxidation tests, the alloys were tested under various testing conditions at

[1] HAYNES, HASTELLOY, 214, 233, HR-224, and 230 are registered trademarks of Haynes International, Inc.

Table 1 Nominal chemical composition of the alloys studied (wt%)

Alloy	Ni	Co	Cr	Al	Si	Ti	Mn	Fe	Mo	W	C	Others
214	Bal	2[a]	16	4.5	0.2[a]	0.5[a]	0.5[a]	3	0.5[a]	0.5[a]	0.04	0.1Zr[a],0.01Y
233	Bal	19	19	3.3	0.2[a]	0.5	0.4[a]	1.5[a]	7.5	0.3[a]	0.1	0.5Ta, 0.03Zr, 0.025Y[a]
HR-224	Bal	2[a]	20	3.8	0.3	0.3	0.5[a]	27.5	0.5[a]	0.5[a]	0.05	0.025Zr[a]
230	Bal	5[a]	22	0.3	0.4	0.1[a]	0.5	3[a]	2	14	0.1	0.02La
188	22	Bal	22	–	0.35	–	1.25[a]	3[a]	–	14	0.1	0.03La
617	Bal	12.5	22	1.2	0.2[a]	0.3	0.2[a]	1	9	–	0.07	–
X	Bal	1.5	22	0.5[a]	1.0[a]	0.15[a]	1[a]	18	9	0.6	0.1	–
625	Bal	1[a]	21	0.4[a]	0.5[a]	0.4[a]	0.5[a]	5[a]	9	–	0.1[a]	3.7Nb

[a]Maximum value

982 and 1093 °C (1800 and 2000 °F), including: (i) static oxidation test with a total 1008h exposure cycled each week (168 h) in flowing air, (ii) 500- or 1000h cyclic oxidation test cycled hourly in flowing air, (iii) 500- or 1000h dynamic oxidation test (burner rig test) cycled every 30 min in high-velocity combustion gas burning fuel oil and air, (iv) one-year (8640 h) long-term oxidation test cycled every 30 days in flowing air, and (v) water vapor oxidation test with a total 1008h exposure cycled each week (168 h) in air + (5–30)% water vapor. 3 L/min air flow was used in the static and cyclic oxidation tests, 500 mL/min flow rate was used in the water vapor oxidation tests, and the high-velocity combustion gas stream had about 0.3 Mach (100 m/s) velocity in the dynamic oxidation tests. For each oxidation cycle, the test coupons were inserted into the hot zone of the furnace at the test temperature and removed from the furnace for air-cooling. High-temperature corrosion tests included nitridation and carburization tests, which were performed in 100% ultra-high purity nitrogen, containing 0.9 ppm O_2 and 2.8 ppm H_2O, and Ar–5%H_2–2%C_3H_6 atmosphere, respectively. The nitridation test was conducted for 1008 h cycled weekly in flowing nitrogen gas at 871 and 982 °C (1600 and 1800 °F), and the carburization test was conducted for 96 h with four 24h cycles at 871 °C (1600 °F). The gas flow rate for the carburization and nitridation tests was 100 mL/min, and after each cycle, the test coupons were furnace-cooled (~4 °C/min) and then rotated to have the coupons exposed at all test locations. The nitridation and carburization test systems were purged with the test gas flow overnight. In the carburization test, the test coupons were brushed to remove carbon soot before weight measurement after each cycle. Weight change, metal loss, internal penetration, and carbon or nitrogen contents were measured to analyze corrosion attack and corrosion behaviors of the alloys tested.

To evaluate overall oxidation attack, Metal Loss, Average Internal Penetration (Avg. Int. Pen.), Maximum Internal Penetration (Max. Int. Pen.), Average Metal Affected (Avg. Met. Aff.), and Maximum Metal Affected (Max. Met. Aff.) were measured to quantify oxide formation, scale spallation, and internal oxidation penetration (Fig. 1). Avg. Met. Aff. is the sum of Metal Loss (Metal Loss (A-B)/2 in Fig. 1) and Avg. Int. Pen. (C in Fig. 1), and Max. Met. Aff. is the sum of Metal Loss and Max. Int. Pen. (D in Fig. 1). The results of Metal Loss and Avg. Met. Aff.

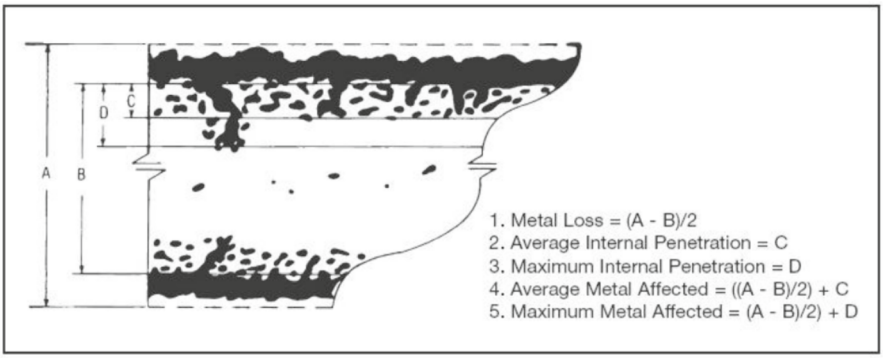

Fig. 1 Methodology used in the present study to evaluate oxidation attack [16] ("A" refers to initial coupon thickness)

are mainly used to evaluate alloy oxidation behaviors in the present paper. For the nitridation and carburization tests, Average Internal Penetration (Avg. Int. Pen.) was used for corrosion evaluation. SEM/EDS (Scanning Electron Microscopy/Energy-Dispersive X-ray Spectroscopy) was used to further characterize oxidation and corrosion attack.

High-Temperature Oxidation Resistance

The results of the static oxidation, cyclic oxidation, and burner rig oxidation tested at 1093 °C are shown in Fig. 2, in which the oxidation attack was evaluated in the terms of Metal Loss and Avg. Met. Aff. With the high-temperature exposure times between 500–1008 h, the oxidation attack results show the severity of the three oxidation tests, *i.e.*, the burner rig test (30min thermal cycling) was the most severe, followed by the cyclic oxidation test (1h thermal cycling) and then the static oxidation test (168h thermal cycling), reflecting the critical effect of thermal cycling, along with the testing atmospheres. Under the three test conditions, the alumina-forming 214 and 233 alloys showed significantly superior oxidation resistance to the

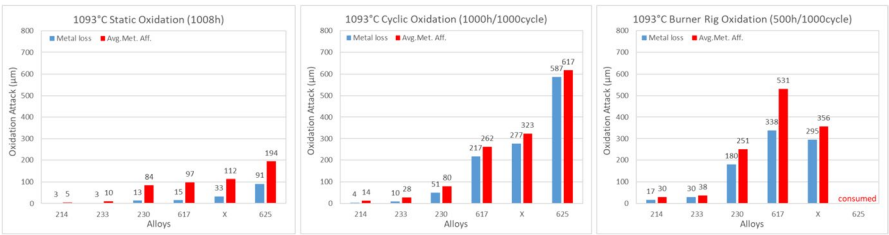

Fig. 2 Static, cyclic, and burner rig oxidation tested at 1093 °C (X and 625 alloys were tested for 500 h/500 cycles in the cyclic oxidation test)

chromia-forming alloys. Please note that Metal Loss is the total metal consumed from oxide scales formed and oxide scales spalled, and no spallation was observed on 214 and 233 alloys during the tests. Although not shown, the excellent oxidation resistance of 214 and 233 alloys was attributed to the formation of a thin alumina scale which was extremely adherent and highly resistant to thermal cycling (up to 30min cycling condition). The oxidation resistance of the chromia-forming alloys varied widely at this extreme test temperature. The chromia-forming alloys showed relatively low Metal Loss, such as scale spallation, and internal penetration was the main oxidation attack in the static oxidation test. While 625, X, and 617 alloys experienced breakaway oxidation in both cyclic and burner rig oxidation tests, and especially, the 625 alloy coupon was consumed in the burner rig test. Based on the oxidation results, the chromia-forming 625, X, and 617 alloys were not able to provide sufficient long-term performance under severe thermal cycling conditions at 1093 °C. Among the chromia-forming alloys, 230 alloy showed the best performance without experiencing breakaway oxidation. The good high-temperature oxidation resistance of 230 alloy has been attributed to its chemical composition and, specifically, the contribution of the reactive element La [17]. However, 230 alloy and the other chromia formers underwent significant oxidation attack when compared to the alumina-forming alloys, and chromia oxidation (Reaction 1) could be a contributing factor.

Figure 3 shows the results of the same alloys after the static oxidation, cyclic oxidation, and burner rig oxidation tests at the lower temperature of 982 °C. The oxidation attack on the alloys tested at this temperature was significantly lower than that tested at 1093 °C, exhibiting the significant effect of temperature. None of the alumina or chromia-forming alloys experienced breakaway oxidation during these ~ 1000h tests under the three oxidation conditions. It is seen that the 1000h cyclic oxidation test with 1h thermal cycling did not result in significantly higher oxidation attack when compared to the static oxidation test (1008 h cycled every 168 h), implying both chromia and alumina scales had good ability to resist scale degradation and spallation under thermal cycling conditions at 982 °C. However, these alloys experienced apparently higher oxidation attack, especially significantly higher Metal Loss, in the 1000h burner rig oxidation test, which could be attributed to more severe cycling, high gas flow velocity, and high-temperature corrosion caused by impurities, such as sulfur, in the fuel combustion atmosphere. At this test

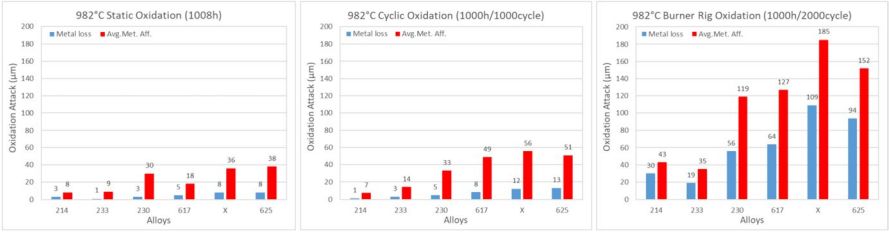

Fig. 3 Static, cyclic, and burner rig oxidation tested at 982 °C (233 alloy was tested for 1000 h/2000 cycles in the cyclic oxidation test)

temperature, the alumina-forming 214 and 233 alloys also showed superior oxidation resistance when compared to the chromia-forming alloys in terms of Metal Loss and Avg. Met. Aff.

The long-term oxidation behavior of an alloy could be different from that of a short-term exposure and cannot be extrapolated from short-term oxidation results. Breakaway oxidation exhibiting an accelerated weight loss is a major material concern for long-term exposures, in which a protective chromia or alumina scale will degrade, spall, and re-heal iteratively, resulting in continuous consumption and depletion of Cr and Al in the alloy. Once the Cr or Al content in an alloy is not sufficient to sustain the re-formation of a protective chromia or alumina scale, faster-growing and less protective oxides will form to trigger breakaway oxidation, i.e., the loss of high-temperature oxidation protection. Long-term oxidation test for a period of 360 days cycled every 30 days at 1093 °C was conducted on the same alloys as tested in Figs. 2 and 3, and their oxidation attack results are presented in Fig. 4. It is noted that the 625 alloy coupon was only tested for 240 days due to severe oxidation wastage. Compared to the static oxidation test results (1008 h at 1093 °C) in Fig. 2, the long-term oxidation results show apparently more severe oxidation attack on the chromia-forming alloys. For example, the Metal Loss of 230, 617, and X alloys after the 360-day (8640 h) exposure was 13–15 times of the Metal Loss after the 1008h exposure, and the 625 alloy experienced breakaway oxidation before the 240-day (5760 h) exposure in the long-term oxidation test. By contrast, the two alumina-forming alloys kept excellent oxidation resistance with low Metal Loss and internal penetration in the long-term oxidation test, especially for 214 alloy. These results are consistent with the long-term oxidation study by Srivastava et al. [18], in which 214, 230, X, and HR-120 alloys were tested for 360 days at 982, 1093, 1149, and 1204 °C. The

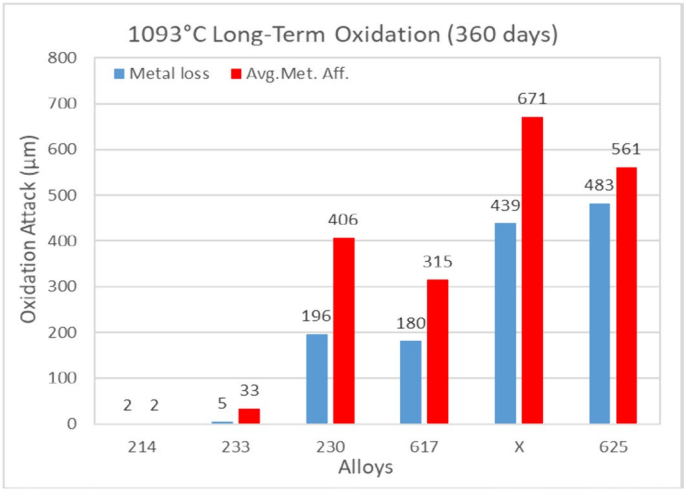

Fig. 4 Long-term 360-day oxidation test at 1093 °C (625 alloy was tested for 240 days due to severe oxidation wastage)

study showed only small weight change and oxidation attack for the four alloys at 982 °C, but the oxidation attack on the chromia-forming 230, X, and HR-120 alloys increased significantly at higher temperatures, e.g., the rate of weight loss increased by an order of magnitude at 1149 °C. In contrast, 214 alloy exhibited a thin and adherent alumina scale resulting in minimal metal loss and internal oxidation penetration up to 1204 °C. In the present study, the reactive elements Zr and Y in 233 and 214 alloys are believed to assist the alloys to form and maintain a protective alumina scale for their excellent long-term oxidation resistance. In another study [17], 233 alloy showed comparable oxidation resistance with 214 alloy when tested at 871, 982, and 1149 °C by forming a protective alumina scale. However, 233 alloy exhibited higher scale growth kinetics than 214 alloy, which was attributed to the formation of Zr-rich oxide particles in the alumina scale formed on 233 alloy.

Eight Ni- or Co-base alloys were exposed in air + (5–30)% water vapor for 1008 h at 982 °C, and the Avg. Met. Aff. results are shown in Fig. 5. It is noted that not every alloy was tested under all conditions. Among the alloys tested, the alumina-forming 214, 233, and HR-224 alloys exhibited superior water vapor oxidation resistance to the chromia-forming alloys in the 5–30% water vapor atmospheres. When comparing to the static oxidation test results in Fig. 3 (tested for 1,008 h in air), it is clearly shown that water vapor increased oxidation attack on the chromia-forming 230, 617, X, and 625 alloys, while the alumina-forming 233 and 214 alloys exhibited similar oxidation attack in the air and air + water vapor oxidation atmospheres. For instance, Avg. Met. Aff. tested in water vapor was about 2.5 times of that tested in air for 617 alloy, reflecting the effects of water vapor on aggravating high-temperature oxidation attack on the chromia-forming alloy. With the increase in water vapor contents, the alumina-forming alloys showed slightly increased oxidation attack with the most oxidation attack observed in air + 30% water vapor. It is noteworthy that the effect of varying water vapor content was not apparent on the chromia alloys, such as similar

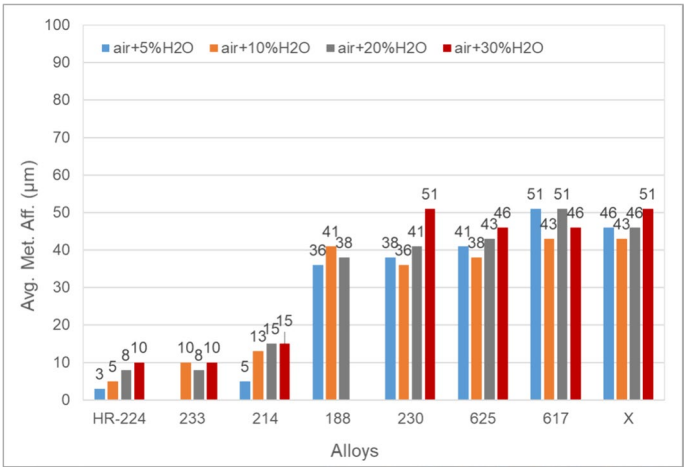

Fig. 5 1008h oxidation tests in air + (5–30)% water vapor at 982 °C

Avg. Met. Aff. observed when exposed to the water vapor contents varying from 5 to 30%, which should be attributed to the combination effects of chromia scale properties and chromia volatilization behaviors at high temperatures.

Although not shown, the chromia-forming alloys experienced weight gain without significant spallation in the water vapor oxidation tests, and their oxidation attack mainly consisted of internal oxide penetration. In another study [19], the chromia-forming 230, 617, and X alloys showed similar oxidation attacks when exposed in air under furnace-cooling condition, in air under air-cooling condition, and in air + 20% water vapor under furnace-cooling condition at 1093 °C. However, the three alloys showed significantly more oxidation attack, mainly consisting of internal penetration, in air + 20% water vapor under air-cooling condition. Accordingly, the rapid cooling, *i.e.*, air-cooling, contributed to higher internal penetration when exposed in the water vapor atmosphere. Similarly, more internal attack was observed in the chromia-forming alloys when exposed to 5–30% water vapor at 982 °C in the present study (air-cooling). The kinetics of internal oxidation are generally found to be diffusion-controlled, and the depth of the internal oxidation zone, ξ, in an alloy can be described by the following kinetics expression [20]:

$$\xi = \left(\frac{2N_o^s D_o t}{\nu N_B^o}\right)^{1/2} \tag{3}$$

where N_o^s is the solubility of the oxidant in the alloy, D_o is the diffusivity of the oxidant in the alloy, N_B^o is the initial solute concentration, ν is the ratio of the oxidant ions to the solute cations in the oxide, and t is the time. The product $N_o^s D_o$ is called the oxygen permeability in the alloy, and N_o^s is controlled by the oxygen partial pressure at the alloy/scale interface. In the present study, the increased internal penetration in the chromia-forming alloys when exposed in the water vapor atmospheres was likely attributed to a greater oxygen permeability from higher value of N_o^s, which was attributed to higher oxygen partial pressure at the alloy/scale interface. Figure 6 shows the cross-sectional SEM/BSE images of 230 alloy after 1008h static air oxidation test (with air-cooling) and air + 30% water vapor oxidation test (with air-cooling) at 982 °C, and it is seen that the chromia scale exhibited significant amounts of

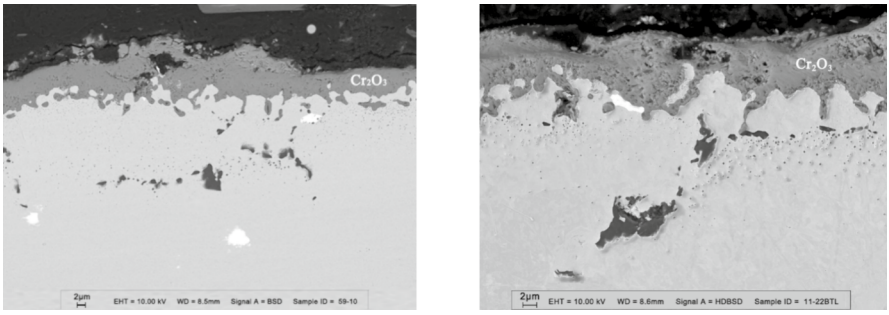

Fig. 6 SEM images of 230 alloy after 1008h oxidation test at 982 °C in air (left) and in air + 30% water vapor (right)

pores and voids in the water vapor oxidation test (the right image in Fig. 6) when compared to that in the air oxidation test (the left image in Fig. 6). In the study of chromia scales grown on pure chromium at 900 °C by Henry et al. [21], porosity was observed within chromia scales that formed in Ar–15%H_2O atmosphere, whereas under dry condition (Ar–15%O_2), porosity was confined to the metal/scale interface. Their study suggested water vapor contributed to the rapid growth of an internal Cr_2O_3 subscale due to probably very mobile hydroxide ions in H_2O, and the subscale was thought to incorporate voids during growth, leading to the formation of porosity. However, the similar oxidation attacks in air (with slow/rapid cooling) and water vapor (with slow cooling) indicated that the effects of porosity were not significant in water vapor under slow cooling condition, and rapid cooling played a critical role in water vapor oxidation [19]. In consistent with the finding, the present study implies that rapid cooling likely promoted the development of pores/voids, fissures, and/or microcracks in chromia scales, which resulted in higher oxygen partial pressure at the alloy/scale interface and subsequent deeper internal oxidation penetration in water vapor atmospheres at high temperatures, such as 982 °C and above; however, its mechanism remains unclear and needs further investigation.

High-Temperature Nitridation Resistance

214, 233, 230, 188, 625, and 617 alloys were tested for 1008 h cycled every 168 h in 100% ultra-high purity nitrogen gas at 871 and 982 °C. The 233 alloy was additionally tested in a pre-oxidized condition (pre-oxide. 233, forming a ~ 0.5μm alumina scale) to check the effectiveness of an alumina scale to resist nitridation attack. To evaluate nitridation attack, nitrogen absorption and the depth of average internal nitridation penetration, *i.e.*, Avg. Int. Pen., were measured. Although not shown, the weight changes of the alloys tested showed parabolic kinetics. The parabolic rate constants were calculated and are listed in Table 2, along with nitrogen absorption

Table 2 High-temperature nitridation test results

Alloy	871 °C nitridation Test			982 °C nitridation test		
	Nitrogen absorption (mg/cm^2)	Avg. Int. Pen. (μm)	Parabolic rate constant, k_p ($g^2cm^{-4}\ s^{-1}$)	Nitrogen absorption (mg/cm^2)	Avg. Int. Pen. (μm)	Parabolic rate constant, k_p ($g^2cm^{-4}\ s^{-1}$)
Pre-oxid. 233	< 0.1	0	7.6×10^{-15}	0.1	0	1.6×10^{-14}
214	0.1	0	1.7×10^{-14}	0.1	0	1.2×10^{-14}
233	0.1	12	1.9×10^{-14}	0.3	193	8.6×10^{-14}
188	0.2	53	3.0×10^{-14}	3.3	389	8.9×10^{-13}
230	0.4	58	1.1×10^{-13}	4.0	312	2.1×10^{-12}
625	0.4	92	1.2×10^{-13}	7.0	450	3.3×10^{-12}
617	0.6	61	1.8×10^{-13}	7.2	765	5.6×10^{-12}

233 alloy without pre-oxidation treatment experienced local internal penetration in both tests

and Avg. In. Pen. results. It is seen that the alumina-forming alloys exhibited significantly lower kinetics, nitrogen absorption, and internal penetration than the chromia-forming alloys tested at the two temperatures. Especially, the 214 and pre-oxidized 233 alloys showed negligible nitridation attack, in terms of nitrogen absorption and internal penetration, at both temperatures, while the 233 alloy coupon without pre-oxidation treatment experienced some local nitridation attack. As for the chromia-forming alloys, 230 and 188 alloys showed better nitridation resistance than 625 and 617 alloys. Based on the oxidation test results in the previous sections, 230 alloy exhibited better oxidation resistance than 617 and 625 alloys, which implies that the chromia scale formed on 230 alloy was more protective to prevent nitrogen penetration. It is noted that 188 alloy showed the lowest kinetics among the chromia-forming alloys, and it was attributed to the formation of a thin silica layer between its chromia scale and substrate. The 617 and 625 alloys contain stronger nitride-forming elements, such as Al and Nb, respectively, which increased the potentials of internal nitride formation. It is noted that the alloys in Table 2 are listed in an ascending order of nitrogen absorption, and the ranking of Avg. Int. Pen. was occasionally different from the nitrogen absorption order. For example, 617 alloy showed the highest nitrogen absorption, but its Avg. Int. Pen. was shallower than that of 625 alloy at 871 °C. This variation in the chromia formers was attributed to their alloy composition and microstructure difference, which affected chromia scale properties, nitrogen diffusion, and internal nitride formation behaviors. The nitridation attack in the chromia-forming alloys was significant at 982 °C, such as an order of magnitude increase in the parabolic rate constant and near 800μm internal nitridation in 617 alloy, indicating chromia scale was not effective to resist nitridation attack at 982 °C and above.

The cross-sectional examination of the tested alloys revealed the formation of an alumina scale on 214 and 233 alloys, while a chromia scale formed on the chromia-forming alloys. For the test nitrogen gas containing ~ 9×10^{-7} atm oxygen impurity, alumina and chromia are thermodynamically favored at the test temperatures. The cross-sectional SEM/BSE images of 214, 625, and 617 alloys after the nitridation test at 871 °C are selected to show their oxide scale and internal nitridation penetration characteristics (Fig. 7). Although not shown, some local areas on the 233 alloy coupon without pre-oxidation treatment showed discontinuities of alumina scale, and accordingly, chromia scale formed at these locations, which was attributed to the alloy's lower Al content (3.3 wt%) when compared to 4.5 wt% Al in 214 alloy.

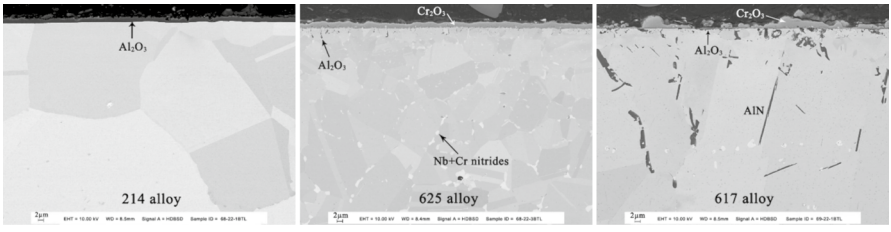

Fig. 7 Cross-sectional SEM/BSE images of 214, 625, and 617 alloys after the nitridation test at 871 °C

In the local areas with chromia scale formation on the 233 alloy without pre-oxidation treatment, internal aluminum nitrides (AlN) precipitated. Apparently, the Al content in 233 alloy was insufficient to rapidly establish a continuous alumina scale due to the slow kinetics of alumina formation and growth in the nitrogen atmosphere. On the other hand, with the establishment of a continuous alumina scale, negligible nitrogen absorption and internal penetration were observed in the 214 and pre-oxidized 233 alloys at both test temperatures, implying highly effectiveness of an alumina scale to resist nitrogen penetration. For the chromia-forming alloys, significant internal nitridation occurred, mainly consisting of chromium nitrides. The 617 and 625 alloys formed very different internal nitrides due to their compositional difference. The 625 alloy containing 3.7%Nb formed NbN precipitates along grain boundaries at both test temperatures. The relatively high Al content in 617 alloy promoted nitrogen absorption and the formation of needle- and plate-shape AlN precipitation. It is noted that even though a very thin alumina layer was observed at the scale/alloy interface as shown in the 617 alloy image in Fig. 7, this alumina layer was likely too thin or not continuous to be effective to suppress nitrogen penetration. The nitridation test results clearly show that an alumina scale is significantly superior to a chromia scale for high-temperature nitridation resistance.

High-Temperature Carburization Resistance

For the carburization test at 871 °C, the activity of carbon, a_c, and equilibrium oxygen partial pressure, p_{O2}, were calculated to be 1 and 6.1×10^{-25} atm, respectively, by using HSC software. Table 3 lists the carbon absorption and average internal carburization penetration (Avg. Int. Pen.) results after the carburization test. It is noted that measurement of internal carburization depth can be very difficult when differentiating carbides forming by carburization from those forming by thermal aging, especially when carburization is not severe or carbide precipitates are very tiny and discrete at carburization penetration front. From the test results, the two alumina-forming alloys, 214 and 233, showed significantly better carburization resistance than the four chromia-forming alloys in both carbon absorption and internal carburization penetration as the result of forming an alumina scale. For the chromia-forming alloys, the carbon absorption order of the alloys is considerably different

Table 3 High-temperature carburization test results at 871 °C

Alloy	Carbon absorption (mg/cm^2)	Avg. Int. Pen. (μm)
214	0.5	<2
233	0.6	47
230	2.3	300
617	3.5	429
188	3.7	307
625	4.3	218

from the order of Avg. Int. Pen. For example, 617 alloy had less carbon absorption than 188 and 625 alloys, but its internal carburization penetration was the deepest in the alloys tested. The difference was attributed to the different carbide formation in these alloys, depending on alloy composition and microstructure. The disagreement between the orders of carbon absorption and internal carburization penetration indicates the sensitivity of criteria to evaluate carburization attack. Internal carbides formed during exposure can severely degrade room temperature ductility and toughness of the alloy, especially in heavy carburization situations [14, 22]. Moreover, internal carbides increase the volume of the carburized zone and, subsequently, develop internal stresses to initiate cracking [9, 14]. Accordingly, more carbon absorption is likely to cause a greater debit in ductility, whereas deeper carburization depth could translate into a greater reduction in effective thickness. To better evaluate alloy performance, it is always beneficial to use multiple criteria to characterize carburization attack.

The optical cross-sectional images of the alloys after the carburization test are shown in Fig. 8. The 214 and 233 alloys showed negligible internal carburization attack, and the precipitates shown in the images were either pre-existing or due to thermal exposure. Alumina scale was observed on the 214 and 233 alloys, which contributed to their excellent carburization resistance due to low carbon permeation through the alumina scale. By contrast, no chromia or other oxide scales were observed on the chromia-forming alloys. The oxygen partial pressure calculated (6.1×10^{-25} atm) supports the alumina scales observed, *i.e.*, the formation of Al_2O_3, while Cr_2O_3 was not thermodynamically favored in this reducing atmosphere. 230 and 188 alloys showed similar carburization attack, such as dispersed carbides and penetration depth, while 625 and 617 alloys showed very different carburization characteristics, such as forming much denser and coarser carbides. The carbides formed in the chromia-forming alloys were mainly of the M_3C_2, M_7C_3, and/or $M_{23}C_6$ types, enriched with Cr, which formed from surface

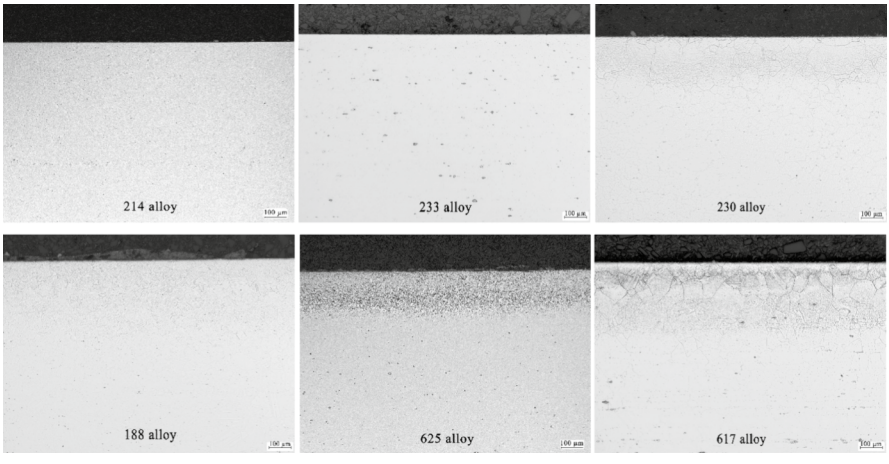

Fig. 8 Optical cross-sectional images of the alloys studied after the carburization test at 871 °C

to matrix with decreasing carbon activity. Mo-rich M_6C carbides were detected in 625 and 617 alloys, and in addition, Nb-rich carbides were found in 625 alloy. For the chromia-forming alloys without the formation of an oxide scale, the internal carburization penetration was controlled by carbon diffusion in the alloy matrix, and the penetration depth is inversely proportional to the concentration of the carbide-forming elements [14]. Accordingly, the strong carbide-forming elements Nb and Mo present in 625 alloy likely contributed to its shallow carburization penetration but higher carbon absorption when compared to 617 alloy.

Summary

The superior high-temperature oxidation and corrosion resistance of alumina scales were demonstrated by the static oxidation, cyclic oxidation, dynamic (burner rig) oxidation, long-term oxidation, and water vapor oxidation tests at 982 and 1093 °C, the nitridation tests at 871 and 982 °C, and the carburization test at 871 °C. The alumina-forming alloys, HAYNES® 214®, 233®, and HR-224® alloys, showed significantly superior oxidation and corrosion resistance to the chromia-forming alloys in the present study. The excellent high-temperature oxidation and corrosion resistance of the alumina-forming alloys were attributed to the formation of a protective alumina scale, which was thin, stable, and adherent to the alloy substrate to be highly resistant to mass penetration and scale spallation. By contrast, the chromia-forming alloys could experience breakaway oxidation under severe cycling condition or during long-term exposure. In water vapor atmospheres, rapid cooling upon cycling likely increased oxygen permeability in the chromia-forming alloys and, accordingly, resulted in deeper internal oxidation penetration. In the reducing carburization atmosphere, an alumina scale formed on the alumina-forming alloys to provide excellent carburization resistance. In the nitridation tests, chromia scales were more susceptible to nitrogen penetration, responding to greater nitridation attack. The nitridation test results between the 233 alloy coupons with and without pre-oxidation treatment, along with that of 214 alloy, clearly showed that the alumina scale was highly effective to suppress nitrogen penetration for the excellent nitridation resistance of the alumina-forming alloys. Accordingly, pre-oxidation treatment of alumina-forming alloys could provide an effective alloy protection method for high-temperature applications under severe corrosion conditions.

Author Contribution B. L. and L.M. P. wrote the main manuscript text, and B. L. prepared the figures and tables. Both authors reviewed the manuscript.

Data Availability No datasets were generated or analyzed during the current study.

Declarations

Conflict of interest The authors declare no competing interests.

References

1. D. Caplan and M. Cohen, *Journal of the Electrochemical Society* **108**, 1961 (438).
2. E. A. Gulbransen and S. A. Jansson, in Heterogeneous Kinetics at Elevated Temperatures, eds. G. R. Belton and W. L. Worrell, (Plenum Press, New York, 1970), p 181.
3. H. C. Graham and H. H. Davis, *Journal of the American Ceramic Society* **54**, 1971 (89).
4. J. W. Brook and P. J. Bridges, *Superalloys* **88**, 1988 (33).
5. S. K. Rhee and A. R. Spencer, *Metallurgical Transactions* **1**, 1970 (2021).
6. E. J. Opila, *Materials Sciences Forum* **461–464**, 2004 (765).
7. N. Birks and F. S. Pettit, *Materials Science Engineering A* **143**, 1991 (187).
8. D. J. Young, *High temperature oxidation and corrosion of metals*, 2nd ed (Elsevier, Oxford, 2016),.
9. G. Y. Lai, *High-temperature corrosion and materials applications*, (ASM International, Almere, 2007).
10. E. J. Opila, N. S. Jacobson, D. L. Myers, and E. H. Copland, *JOM* **58**, 2006 (22).
11. D. P. Whittle, J. Stringer, and J. Phil, *Philosophical Transactions of the Royal Society of London. Series A, Mathematical and Physical Sciences* **295**, 1980 (309).
12. P. Y. Hou, *Materials Science Forum* **696**, 2011 (39–44).
13. J.J. Barnes and G.Y. Lai, High Temperature Nitridation of Fe-, Ni- and Co-base Alloys, Proceeding of Corrosion and Particle Erosion at High Temperatures, TMS/AIME conference, Las Vegas, NV, Feb. 26 - Mar. 2, 1989.
14. H. J. Grabke, Carburization – A high Temperature Corrosion Phenomenon, MTI Publication No. 52, Materials Technology Institute, 1998.
15. G.Y. Lai and M.F. Rothman, High-Temperature Alloys for Application in Carburizing Environments, Paper 11, Corrosion/84 annual conference, NACE, April 2–6, 1984.
16. F.G. Hodge, High Performance Alloys Solve Problems In The Process Industries, Paper 173, Corrosion/91 annual conference, NACE, 1991.
17. B. Li, L.M. Pike, V. Deodeshmukh, and S.K. Srivastava, High Temperature Oxidation Resistance of a Newly Developed Ni-Based Alumina-Forming NiCoCrMoAl Alloy, Paper C2021–16537, Corrosion 2021 annual conference, AMPP, 2021.
18. S.K. Srivastava, M.J. Newburn, J.P. Cotner and M.A. Richeson, Long-term oxidation behavior of selected high temperature alloys, Paper GT2007–28269, Proceedings of GT2007 ASME Turbo Expo 2007: Power for Land, Sea and Air, 2007: 171.
19. B. Li, V. Deodeshmukh, and L.M. Pike, Oxidation Resistant Behaviors of Commercial High Temperature Alloys in the Atmospheres Containing Water Vapor, Paper C2024–20729, AMPP 2024 annual conference, New Orleans, LA, March, 2024.
20. N. Birks and G.H. Meier, Introduction to High Temperature Oxidation of Metals, Edward Arnold, 1983.
21. S. Henry, J. Mougin, Y. Wouters, J.-P. Petit, and A. Galerie, *Materials at High Temperatures* **17**, 2000 (231).
22. J. Klower and U. Heubner, *Materials and Corrosion* **49**, 1998 (237).

Authors and Affiliations

Bingtao Li[1] · Lee M. Pike[1]

✉ Bingtao Li
bli@haynesintl.com

Lee M. Pike
lpike@haynesintl.com

[1] Research and Technology Department, Haynes International, Inc., 1020 West Park Ave, Kokomo, IN 46904, USA